Transcriptomic analysis reveals key lncRNAs associated with ribosomal biogenesis and epidermis differentiation in head and neck squamous cell carcinoma[*#]

Yu-zhu GUO[1], Hui-hui SUN[1], Xiang-ting WANG[1], Mei-ting WANG[†‡1,2]

[1]School of Life Sciences, University of Science and Technology of China, Hefei 230026, China
[2]College of Liren, Yanshan University, Qinhuangdao 066004, China
[†]E-mail: stucomputer0@163.com
Received June 25, 2017; Revision accepted Feb. 26, 2018; Crosschecked Aug. 14, 2018

Abstract: Objective: In this study, we aimed to expand current knowledge of head and neck squamous cell carcinoma (HNSCC)-associated long noncoding RNAs (lncRNAs), and to discover potential lncRNA prognostic biomarkers for HNSCC based on next-generation RNA-seq. Methods: RNA-seq data of 546 samples from patients with HNSCC were downloaded from The Cancer Genome Atlas (TCGA), including 43 paired samples of tumor tissue and adjacent normal tissue. An integrated analysis incorporating differential expression, weighted gene co-expression networks, functional enrichment, clinical parameters, and survival analysis was conducted to discover HNSCC-associated lncRNAs. The function of *CYTOR* was verified by cell-based experiments. To further identify lncRNAs with prognostic significance, a multivariate Cox proportional hazard regression analysis was performed. The identified lncRNAs were validated with an independent cohort using clinical feature relevance analysis and multivariate Cox regression analysis. Results: We identified nine HNSCC-relevant lncRNAs likely to play pivotal roles in HNSCC onset and development. By functional enrichment analysis, we revealed that *CYTOR* might participate in the multistep pathological processes of cancer, such as ribosome biogenesis and maintenance of genomic stability. *CYTOR* was identified to be positively correlated with lymph node metastasis, and significantly negatively correlated with overall survival (OS) and disease free survival (DFS) of HNSCC patients. Moreover, *CYTOR* inhibited cell apoptosis following treatment with the chemotherapeutic drug diamminedichloroplatinum (DDP). *HCG22,* the most dramatically down-regulated lncRNA in tumor tissue, may function in epidermis differentiation. It was also significantly associated with several clinical features of patients with HNSCC, and positively correlated with patient survival. *CYTOR* and *HCG22* maintained their prognostic values independent of several clinical features in multivariate Cox hazards analysis. Notably, validation either based on an independent HNSCC cohort or by laboratory experiments confirmed these findings. Conclusions: Our transcriptomic analysis suggested that dysregulation of these HNSCC-associated lncRNAs might be involved in HNSCC oncogenesis and progression. Moreover, *CYTOR* and *HCG22* were confirmed as two independent prognostic factors for HNSCC patient survival, providing new insights into the roles of these lncRNAs in HNSCC as well as clinical applications.

Key words: Head and neck squamous cell carcinoma; Long noncoding RNA (lncRNA); Weighted gene co-expression network analysis (WGCNA); Clinicopathological feature; Multivariate Cox regression model

https://doi.org/10.1631/jzus.B1700319   **CLC number:** Q522

1 Introduction

Head and neck squamous cell carcinoma (HNSCC), the sixth leading cancer worldwide, is characterized by phenotypic, aetiological, biological, and clinical heterogeneity (Leemans et al., 2011). Several factors and clinical features have been implicated to be predictive for HNSCC development, including age, sex, smoking, alcohol, tumor stage, nodal status, and human papillomavirus (HPV) status. However, the prognosis of HNSCC patients is still a formidable challenge on account of distant metastasis, therapeutic resistance, or invasive recurrence, which frequently results in a lethal malignancy (Seiwert et al., 2007; Gold et al., 2009). A thorough understanding of HNSCC pathogenesis and the identification of new disease markers would be extremely useful for selecting suitable therapeutic regimens and improving the prognosis of HNSCC patients (Pritzker, 2015).

Long noncoding RNAs (lncRNAs), a class of noncoding RNAs with a length greater than 200 nucleotides, generally exert a regulatory function at the RNA level. Accumulating evidence suggests that lncRNAs play critical roles in almost every aspect of cell biology, including carcinogenesis (Cheetham et al., 2013; Huarte, 2015; Bartonicek et al., 2016; Schmitt and Chang, 2016; Schmitt et al., 2016). This makes lncRNAs a hot target for translational medicine (Salyakina and Tsinoremas, 2016) in addition to microRNAs and transcription factors (Salazar et al., 2014; Miller et al., 2015; Yan et al., 2016). Taking HOX transcript antisense RNA (*HOTAIR*) as an example, the best known regulatory mechanism of this lncRNA is to act as a scaffold molecule and form a complex with Polycomb repressive complex 2 (*PRC2*) to modulate the H3K27me3 level of downstream target genes (Tsai et al., 2010). *HOTAIR* is highly overexpressed in almost all tested cancer types, and functions as an oncogene in cultured cells (Geng et al., 2011; Kim et al., 2013; Li DD et al., 2013; Li X et al., 2013; Hajjari and Salavaty, 2015). Recently, we conducted a meta-analysis, and clarified that *HOTAIR* is positively correlated with tumor development and negatively correlated with clinical outcomes (Min et al., 2017). However, the number of lncRNAs is vast. Currently, the GENCODE project has collected about 16 000 lncRNAs, and this number is still climbing due to the development of more robust and sensitive techniques. *HOTAIR* and other functionally characterized lncRNAs represent only a very small proportion of the total number of annotated lncRNAs (Quek et al., 2015; Signal et al., 2016). Therefore, our knowledge of the majority of lncRNAs remains elusive.

The advancement of RNA sequencing and computational techniques over the past decade has facilitated the generation of rich and diverse information about lncRNAs. Previous transcriptome analyses identified numerous dysregulated lncRNAs which play regulatory roles in multiple cellular processes such as genomic mutation and DNA methylation. However, these studies were either based on microarray analysis focusing on a particular type of HNSCC such as oral squamous cell carcinoma (OSCC) (Zhang et al., 2015) and tongue squamous cell carcinoma (TSCC) (Yu et al., 2017), or based on a relatively small number of HNSCC samples (426 RNA-seq) and lncRNA molecules (500 lncRNAs) (de Lena et al., 2017). In this work, we focused on a more comprehensive dataset with a 28% larger sample size and 2787 lncRNAs. We subsequently performed an integrated transcriptomic analysis incorporating differential expression, weighted gene co-expression networks, functional enrichment, clinical parameters, survival analysis, and a multivariate Cox regression model on 546 RNA-seq datasets, aiming to uncover potential HNSCC-associated lncRNAs and demonstrate their functional roles, and reveal their prognostic signature for patient survival, followed by validation using an independent cohort.

2 Materials and methods

2.1 Data source

The Cancer Genome Atlas (TCGA; http://cancergenome.nih.gov) is a comprehensive and coordinated effort to accelerate our understanding of the molecular basis of cancer through the application of genome analysis technologies. Here, we downloaded level 3 RNA-seq data and clinical data of corresponding patients from the TCGA via Genomic Data Commons (GDC; https://portal.gdc.cancer.gov). In total, there were 546 RNA-seq datasets from 501 patients, including data from 43 paired samples from tumor tissue and adjacent normal tissue. From one patient, only a normal tissue sample was available.

Two types of expression data were used in this study: upper quartile normalized fragments per kilobase per million mapped reads (FPKM-UQ), and raw counts calculated with HTSeq-count (Anders et al., 2015). Genes in the expression profile table had been annotated with Ensembl gene ID (Aken et al., 2016; Yates et al., 2016) by TCGA. All genes were annotated using BioMart (Kinsella et al., 2011), and lncRNAs were then confirmed with GENCODE annotation (Derrien et al., 2012; Harrow et al., 2012; https://www.gencodegenes.org, Version 26).

2.2 Differential expression analysis

The R platform (https://www.r-project.org, Version 3.32) was adopted for data manipulation and statistical analysis (R Development Core Team, 2011). Differential expression analysis was performed using R package edgeR (Version 3.16.5) (Robinson et al., 2010; McCarthy et al., 2012) based on the 43 paired samples (43 tumor tissue samples and 43 adjacent normal tissue samples). Genes with a count per million reads (CPM) (Law et al., 2014) higher than 1 in more than 10 samples were selected for the following analyses. Briefly, Ensembl gene IDs were annotated to gene symbol and Entrez gene IDs to facilitate the following functional profiling. The Benjamini-Hochberg (BH) method was used to correct the P value to a false discovery rate (FDR) for multiple comparisons (Benjamini and Hochberg, 1995). Genes with $\log_2$ fold change ($\log_2 FC$) ≥ 1 and FDR≤ 0.05 were considered as significantly up-regulated, while those with $\log_2 FC \leq -1$ and FDR≤ 0.05 were counted as significantly down-regulated.

2.3 Co-expression network analysis

WGCNA (Langfelder and Horvath, 2008) is a widely used R package for performing weighted gene co-expression network analysis. It transforms gene expression profiles into functional co-expressed gene modules to provide deep insight into the genetic network (Liu R et al., 2015). In our study, all 546 RNA-seq samples and the top 20 000 most abundant genes that accounted for 99.6% of total reads in terms of FPKM-UQ were used in the co-expression network analysis. Low-abundance genes were eliminated as their abundance tends to be highly biased. To construct a more robust network, we applied the bi-weight mid-correlation (bicor) method which is insensitive to

outliers for computing the correlation (Song et al., 2012). For a given gene, the soft degree is defined as the sum of connection weights with other network genes. In network analysis, hub genes are the highly connected genes. By scale-free topology fitting of the network, six was determined to be the best soft threshold power (Fig. S1). Finally, Cytoscape software was employed for visualizing and analyzing the co-expression network (http://www.cytoscape.org, Version 3.4.0; Kohl et al., 2011).

2.4 Geneset enrichment analysis

R package clusterProfiler (Yu et al., 2012) was used to perform the enrichment analysis of cancer hallmark gene ontology (GO), and the Kyoto Encyclopedia of Genes and Genomes (KEGG) for the co-expression network gene modules and hub lncRNA-connected genes (weight ≥ 0.01). The "gmt" files of cancer hallmark gene sets were obtained from the Molecular Signatures Database (MSigDB) on the Gene Set Enrichment Analysis (GSEA) website (http://software.broadinstitute.org/gsea/msigdb; Subramanian et al., 2005). Reduce visualize gene ontology (REVIGO) was adopted to summarize the enriched GO terms in line with their semantic similarity (http://revigo.irb.hr; Supek et al., 2011). All gene set enrichment analyses were carried out using Fisher's exact test based on a hypergeometric distribution, and P values were corrected using the BH method for multiple comparisons. Gene sets or functions with FDR≤ 0.05 were considered significantly enriched.

2.5 Clinical pathological parameters and survival analysis

The association between the expression of each candidate lncRNA and the clinicopathological features of the HNSCC patients was analyzed by calculating the odds ratio (OR) value in terms of a 95% confidence interval (CI) (http://www.medcalc.org/calc/odds_ratio.php; Parshall, 2013). The analyzed clinicopathological parameters included sex (male versus female), age (<65 versus $\geq$65 years old), alcohol habit, smoking history, clinical stage (I/II versus III/IV), tumor size (T1/T2 versus T3/T4), the absence or presence of regional lymph node metastasis, and the absence or presence of distant metastasis (M0 versus M1). Patients with clinical stage IV A, B, or C tumors were classified as "Stage IV". Patients

with tumor size stage T4, T4a, or T4b were classified as "T4". For smoking history, patients categorized as "current smoker" or "current reformed smoker for ≤15 years" were classified as "recent smokers", while those categorized as "current reformed smoker for >15 years" were classified as "reformed smokers". Patients with no information available for a given characteristic were filtered from the corresponding analysis.

The R package survival (Therneau, 2017) was used for survival analysis, and multivariate Cox proportional hazards for regression analysis. The Kaplan Meier (KM) curve was visualized with R package survminer (Kassambara and Kosinski, 2017). Multivariate Cox proportional hazards analysis was conducted to evaluate the independence of the prognostic signature of the hub lncRNAs. The hazard ratio (HR), corresponding 95% CI, and P value were calculated. In total, 500 patients with RNA-seq data for cancer tissue (marked as 01 in the sample ID) were used in survival analysis. The FPKM-UQ value of genes was used to divide the patients into a low expression group and a high expression group based on the lower and upper quartiles, respectively. The difference in the survival distributions of the two groups was tested using a log-rank test with a significance level of 0.05. For the multivariate Cox regression model, the gene expression group and other covariates including sex, age, alcohol habit, smoking history, tumor size, node metastasis, and primary tumor site were included. Covariates with $P \leq 0.05$ were marked as statistically significant in relation to patient survival. The HPV data were not included in the analysis above because most patients did not have this information in TCGA database ((16.48±1.86)% of total upper and lower quartile samples for HPV status, and (20.39±2.41)% for HPV p16).

2.6 Validation using an external dataset

An independent dataset (Rickman et al., 2008) with 81 HNSCC patients from the Oncomine database was used to validate the clinical relevance of the potential HNSCC-associated lncRNAs discovered based on TCGA dataset. Oncomine (https://www.oncomine.org/resource/main.html) collects biological data from a large number of microarrays and allows the users to investigate using clinical-based and pathology-based analyses (Rhodes et al., 2004).

Clinical parameters, overall survival (OS), and multivariate Cox regression analysis adjusting for sex, age, pathological stage (I/II versus III/IV), tumor size, node metastasis, and differentiation (poor, moderate, and well) were considered in this study to validate our findings. Due to the small sample size of this dataset, the median of the expression value was used to divide patients into a high expression group and a low expression group. The chi-squared test was used in the analysis of the association between gene expression group and differentiation. DFS information was not available for this dataset and hence was not analyzed. In total, 79 patients were used for survival analysis because the vital status of two patients was unavailable.

2.7 Cell culture and DDP treatment

TSCC15 cells were purchased from the American Type Culture Collection (ATCC) and cultured following the official instructions. A final concentration of 5 µg/ml cisplatin (diamminedichloroplatinum (DDP), Qilu Pharmaceutical, China) was added to the TSCC15 cells for DNA damage induction.

2.8 RNA interference and transfection

Small interfering RNAs (siRNAs) targeting human *CYTOR* transcript were purchased from RiboBio Co., Ltd. (Guangzhou, China). The siRNA sequences were as follows: siCYTOR-1 (5'-GAAACAGGAA GCTCTATGA-3'), siCYTOR-2 (5'-CACACTTGAT CGAATATGA-3'), and siCYTOR-3 (5'-CCAGTC TCTATGTGTCTTA-3'). Cells were pre-seeded on 6-well plates at a density of 5×10^5 per dish the day before transfection. The negative control or 5 µl of siRNAs were transfected into TSCC15 cells using lipofectamine 3000 (Invitrogen, USA) following the manufacturer's instructions.

2.9 RT-PCR and quantitative RT-PCR

After twice washing with pre-chilled phosphate-buffered saline (PBS), cultured cells were lysed with TRIzol reagent (Ambion, USA). Total RNA was then extracted according to the manufacturer's instructions. The first-strand complementary DNA (cDNA) was synthesized using a HiScript II 1st Strand cDNA synthesis kit (Vazyme, China), with RNA treated with DNase I (Thermo Scientific, USA) as a template. For quantitative polymerase chain reaction (qPCR), the cDNA was analyzed on a LightCycler® 96 (Roche,

Switzerland) using a SYBR Green qPCR kit (Vazyme, China). The relative expression level of the desired lncRNA was calculated by the $2^{-\Delta\Delta C_{T}}$ method normalized to 18S. Primer sequences were as follows: *CYTOR* (F: 5'-AAAATCACGACTCAGCCCCC-3'; R: 5'-AATGGGAAACCGACCAGACC-3'), 18S (F: 5'-GTAACCCGTTGAACCCCATT-3'; R: 5'-CCAT CCAATCGGTAGTAGCG-3'). The expression level was denoted as the mean±standard error of the mean (SEM) of three independent experiments. Differences in expression levels were tested using a two-tailed Student's *t*-test with GraphPad Prism (Version 6.00, La Jolla, California, USA). *P*≤0.05 was considered significant.

2.10 Apoptosis analysis and EdU proliferation assay

TSCC15 cells were transfected with small interfering CYTORs (siCYTORs) or siRNA control for 24 h. Cells were then treated with indicated doses of DDP (5 µg/ml). TSCC15 cells were harvested by trypsinization and washed with PBS. The 1×10^{5} cells were harvested and an FITC Annexin-V apoptosis detection kit (BD Biosciences, USA) was used according to the manufacturer's instructions. A Cellometer Vision image cytometer (Nexcelom Bioscience, USA) was used for apoptosis detection. Data were analyzed using FCS4 Express Cytometry software (De Novo Software, USA). Cell proliferation was assessed using a Cell-Light™ EdU Apollo567 in vitro kit (RiboBio, Guangzhou, China), according to the manufacturer's instructions.

2.11 Cell migration assay and scratch wound healing assay

First, *CYTOR* in TSCC15 cells was knocked down for 24 h. For the cell migration assay, an 8 µm-pore polycarbonate membrane was used to divide transwell chambers into upper and lower chambers. The 1×10^{5} TSCC15 cells re-suspended with 200 µl serum-free medium were added to the upper chamber, and the medium containing 10% fetal bovine serum (FBS) was added to the lower chamber before both chambers were incubated at 37 °C in 5% CO_2 for 24 h. After removing non-migrated cells on the upper side of the membrane using a cotton swab, the membrane was fixed with 95% ethanol for 30 min and stained with 0.25% (2.5 g/L) crystal violet (Sangon, China).

The migrated cells were counted using light microscopy (4×). For the wound healing assay, cells were cultured in 6-well plates and incubated until 100% confluence. Uniform scratches were made using a 200-µl pipette tip, then cells were washed using 1× PBS, which finally was replaced with serum-free medium. The cells from a consistent field in each well were photographed at 0, 24, and 48 h. The migration distance was assessed using Image-pro Plus Version 6.0 (Media Cybernetics, USA).

3 Results

3.1 Overview of this study

Firstly, we obtained clinical data and level 3 RNA-seq data from TCGA. A hierarchical clustering based on the gene expression profile suggested that there was no significant batch effect between samples under different batch operating conditions including BatchID, PlateID, Ship Date, and Tissue Source Site (Fig. S2). Subsequently, differential expression analysis was conducted, followed by the construction of a co-expression network which identified nine HNSCC-related lncRNAs. We then performed functional enrichment analyses on these nine lncRNAs to discover their potential functions and interpret their roles in HNSCC. Six of these nine lncRNAs were shown to be significantly associated with clinical parameters in terms of the OR value. Survival analysis showed that two of these six lncRNAs were significantly associated with the survival of HNSCC patients. Multivariate Cox regression models were used to assess the contribution of these lncRNAs to OS and DFS. The prognostic signature and biological roles of these lncRNAs were validated either on an independent cohort or by laboratory experiments. The workflow of this study is illustrated in Fig. S3.

3.2 Transcriptional profile in tumor tissue

To unearth the gene expression shifts and functional alterations between cancer tissue and its adjacent normal tissue, we performed a differential expression analysis. In total, among 15 851 genes with a CPM past the cutoff described in the methods section, 1385 (8.74%) were identified as significantly up-regulated, and 1956 (12.34%) were down-regulated (Fig. 1a, Table S1). Among those, 78 lncRNAs were
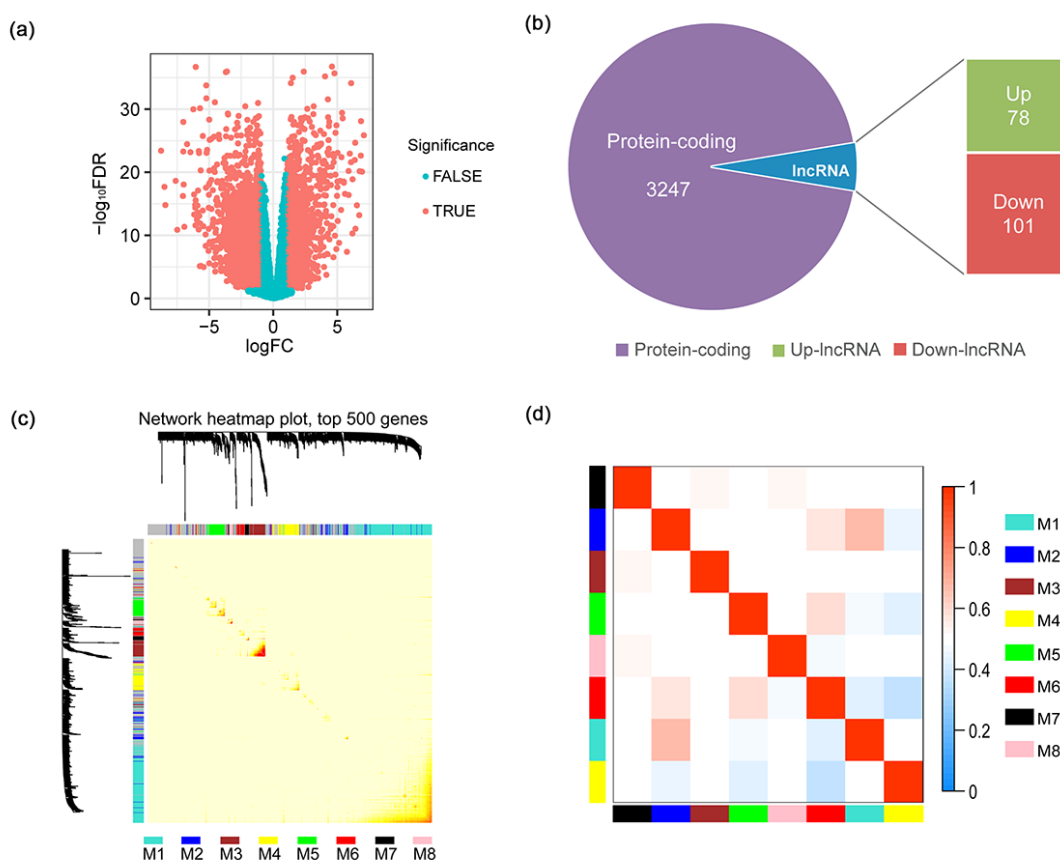
Fig. 1 Functional gene modules detected by co-expression network analysis

(a) The volcano plot shows the magnitude of differential expression between cancer tissue and its adjacent normal tissue. Each dot represents one gene, and genes in read are significantly altered. FDR: false discovery rate; logFC: $\log_2$ fold change. (b) Pie chart shows the proportion of dysregulated lncRNAs in all differentially expressed genes. (c) Topological overlap heatmap of the gene co-expression network. Each row and column represents a gene. Light color indicates low topological overlap, and on the contrary dark color denotes high topological overlap. The different side colors indicate different modules. The dendrogram suggests the clustering of these genes based on the similarity of their gene expression profiles. (d) The correlation between each module demonstrated based on eigengene. Blue represents a negative correlation, while red represents a positive correlation (Note: for interpretation of the references to color in this figure legend, the reader is referred to the web version of this article)

up-regulated, and 101 lncRNAs were down-regulated (Fig. 1b, Table S1). The top 10 most differentially expressed lncRNAs are listed in Table S1. *HCG22* was the most down-regulated lncRNA ($\log_2FC=-5.96$, FDR=1.98×10^{-15}), implicating that it may be highly associated with HNSCC.

3.3 Eight distinct functional gene modules detected by co-expression network analysis

By co-expression network construction and analysis using WGCNA, we obtained eight distinct modules, namely M1 (turquoise), M2 (blue), M3 (brown), M4 (yellow), M5 (green), M6 (red), M7 (black), and M8 (pink), in terms of the WGCNA conventions (Zhang and Horvath, 2005). There were 7301 genes that could not be assigned to any module. A module represents a cluster of highly interconnected genes (Zhang and Horvath, 2005). M1 was the largest module, consisting of 5624 genes (Table S2). As illustrated in the topological overlap matrix (TOM) plot of 500 genes with the high soft degree across all modules (Fig. 1c), M3 had the highest cohesion within the module, but the lowest coupling to other modules. Moreover, correlations between eigengenes of each module showed that M1 and M2 were highly related (Fig. 1d). Among these eight modules, M4 contained the most differentially regulated lncRNAs (Table S2).

3.4 Functional analysis of the modules identified by WGCNA

To gain further biological insights into these modules, we performed GO term enrichment analysis. Genes from M1 are enriched primarily in ncRNA processing, ribosome biogenesis, mitochondrial translation, DNA replication, apoptotic signaling pathways, and DNA damage response (Fig. S4a, Table S2). Genes in M3 are involved mainly in muscle cell development, response to oxygen levels, response to hypoxia, and response to decreased oxygen levels (Fig. S4b, Table S2). The most significantly represented biological processes for M4 genes are keratinocyte differentiation, epidermis development, skin development, and epidermal cell differentiation (Fig. S4c, Table S2). These related biological processes have been widely reported to be associated with tumorigenesis or cancer development (Bartkova et al., 2005; Zaidi et al., 2011; Liu BD et al., 2015).

3.5 Potential cancer-associated lncRNAs revealed by co-expression network analysis

Subsequently, we discovered nine HNSCC-associated hub lncRNAs which were differentially regulated in terms of differential expression analysis ($|\log_2FC|{\geq}1$, $\log_2CPM{>}0$, and FDR${\leq}0.05$) with a soft degree above 10, namely *LINC01372*, *CYTOR*, *SNHG9*, *MAGI2-AS3*, *PICSAR*, *HOTAIRM1*, *FALEC*, *LOC101928844*, and *HCG22* (Table S2). To investigate the potential functions of these hub lncRNAs, and gain a deeper understanding of their roles in HNSCC, we performed gene set enrichment analyses including cancer hallmarks, GO terms, and KEGG pathways based on the genes connected to each lncRNA. Cancer hallmarks enrichment analysis revealed that *CYTOR*, *PICSAR*, *HOTAIRM1*, and *SNHG9* are significantly involved in oxidative phosphorylation,

DNA repair, and *MYC* targets v1 (v2) (Table 1, Table S3). Notably, *SNHG9* belongs to the M2 module which is highly connected to M1, implying they have similar biological functions. Among these four lncRNAs, some have been demonstrated to be related to tumor progression (Gabay et al., 2014). For example, *CYTOR*, which was up-regulated in our data, has also been reported to be overexpressed in gastric cancer and to affect DNA damage, cell cycle arrest, and tumor metastasis (Zhao et al., 2015; Chen et al., 2016). *LINC01372* and *MAGI2-AS3* are associated mainly with cancer hallmarks of myogenesis (Table 1, Table S3), which play essential roles in tumorigenesis (Lamouille et al., 2014; LeBleu et al., 2014). *LOC101928844* and *FALEC* are especially associated with estrogen response (Table 1, Table S3).

GO term enrichment analyses indicated that *CYTOR*, *PICSAR*, *HOTAIRM1*, and *SNHG9* are associated mainly with ncRNA processing, ribosomal RNA (rRNA) processing, ribosome biogenesis, or oxidative phosphorylation (Fig. 2a, Table S4). A number of apoptosis and DNA damage related GO terms were also enriched in *CYTOR*-connected genes, suggesting that *CYTOR* plays a role in these functions (Table 2). *LINC01372* and *MAGI2-AS3* are particularly associated with muscle development and response to oxygen levels (Fig. 2b, Table S4). *HCG22*, *LOC101928844*, and *FALEC* are involved mainly in epidermis development, keratinocyte differentiation, epidermal cell differentiation, and keratinization (Fig. 2c, Table S4). Most of these lncRNAs have not been characterized or well investigated in HNSCC, and some have not previously been reported in cancer studies. Hence, these new findings provide a deeper insight into the roles of these uncharacterized lncRNAs in HNSCC, and importantly provide more knowledge regarding the pathogenesis of HNSCC.

Table 1 Cancer hallmarks enriched in HNSCC-associated hub lncRNAs

Gene symbol	ENSG number	Module	Cancer hallmarks
CYTOR	ENSG00000222041	M1 (turquoise)	Oxidative phosphorylation,
PICSAR	ENSG00000275874		DNA repair,
HOTAIRM1	ENSG00000233429		*MYC* targets v1 (v2)
SNHG9	ENSG00000255198	M2 (blue)	
LINC01372	ENSG00000235475	M3 (brown)	Myogenesis
MAGI2-AS3	ENSG00000234456		
LOC101928844	ENSG00000267709	M4 (yellow)	Estrogen response early
FALEC	ENSG00000228126		
HCG22	ENSG00000228789		N/A

ENSG: the Ensign Group, Inc.; N/A: not applicable

Table 2 List of enriched DNA damage or apoptosis related GO terms for *CYTOR*

| GO ID	GO term	Count	Background	FDR
GO:0042769	DNA damage response, detection of DNA damage	9	36	4.44×10^{-4}
GO:0008637	Apoptotic mitochondrial changes	16	123	2.02×10^{-3}
GO:2001244	Positive regulation of intrinsic apoptotic signaling pathway	8	51	2.49×10^{-2}
GO:2001235	Positive regulation of apoptotic signaling pathway	17	180	3.77×10^{-2}
GO:0043281	Regulation of cysteine-type endopeptidase activity involved in apoptotic process	19	216	4.75×10^{-2}
GO:2001242	Regulation of intrinsic apoptotic signaling pathway	15	155	4.99×10^{-2}
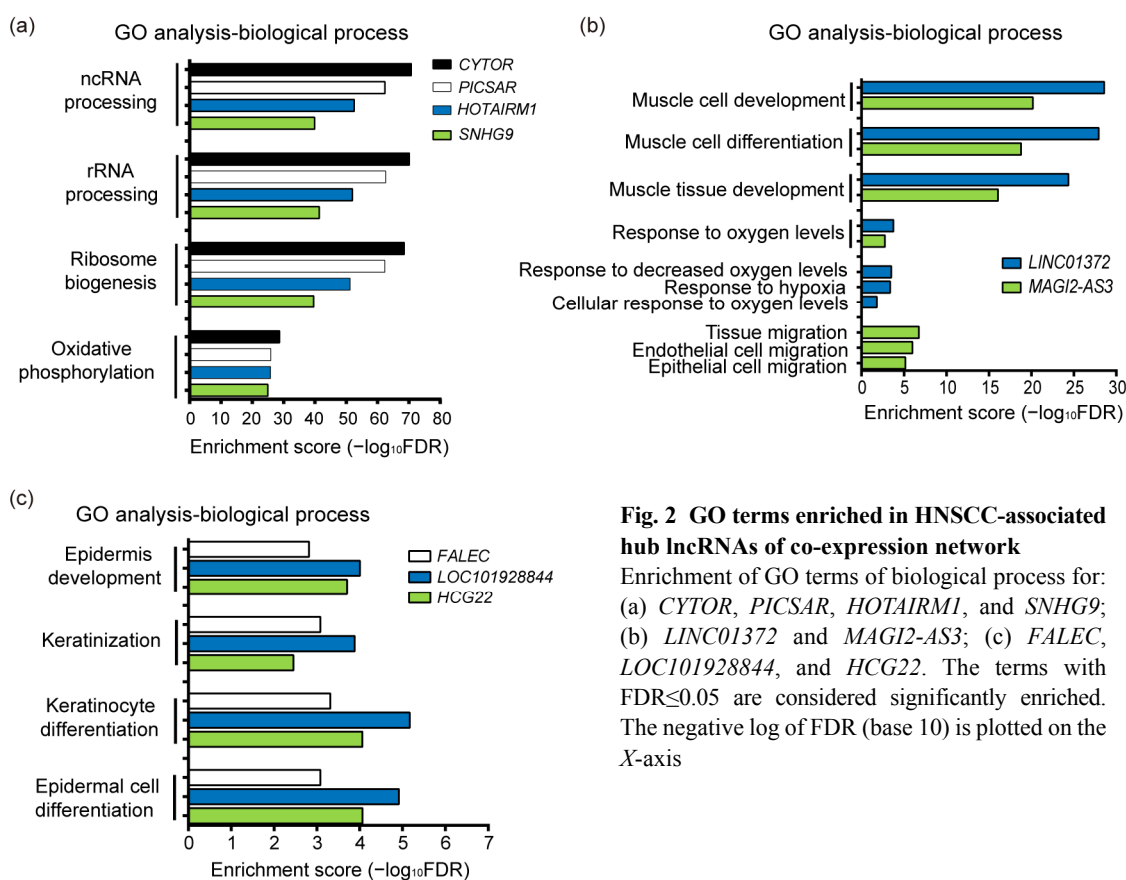
Fig. 2 GO terms enriched in HNSCC-associated hub lncRNAs of co-expression network

Enrichment of GO terms of biological process for: (a) *CYTOR*, *PICSAR*, *HOTAIRM1*, and *SNHG9*; (b) *LINC01372* and *MAGI2-AS3*; (c) *FALEC*, *LOC101928844*, and *HCG22*. The terms with FDR≤0.05 are considered significantly enriched. The negative log of FDR (base 10) is plotted on the *X*-axis

To comprehensively mine the biological roles of these hub lncRNAs, KEGG pathway enrichment analysis was performed using R package clusterProfiler. Fig. 3 and Table S5 list all significantly enriched KEGG pathways with FDR≤0.05 and gene counts ≥5. We discovered that *CYTOR*, *HOTAIRM1*, *PICSAR*, and *SNHG9* are involved primarily in ribosome bio-genesis and maintenance of genomic stability, and that their dysregulation is connected with a predisposition to multiple diseases. The significantly enriched pathways of *MAGI2-AS3* are several cancer-associated signaling pathways such as, cell migration and cell adhesion pathways (extracellular matrix (ECM)-receptor interaction, Gap junction, and Rap1 signaling pathways), angiogenesis signaling pathways (vascular smooth muscle contraction and apelin signaling pathways), and the phosphatidylinositol 3-kinase (PI3K)/Akt signaling pathway. Notably, the functions of enriched pathways are consistent with the observations from GO terms and cancer hallmarks. *LINC01372* appears to be relevant to multiple signaling pathways as well, such as metabolism pathways (glycolysis/gluconeogenesis and oxidative phosphorylation), the hypoxia signaling pathway (FoxO signaling pathway),
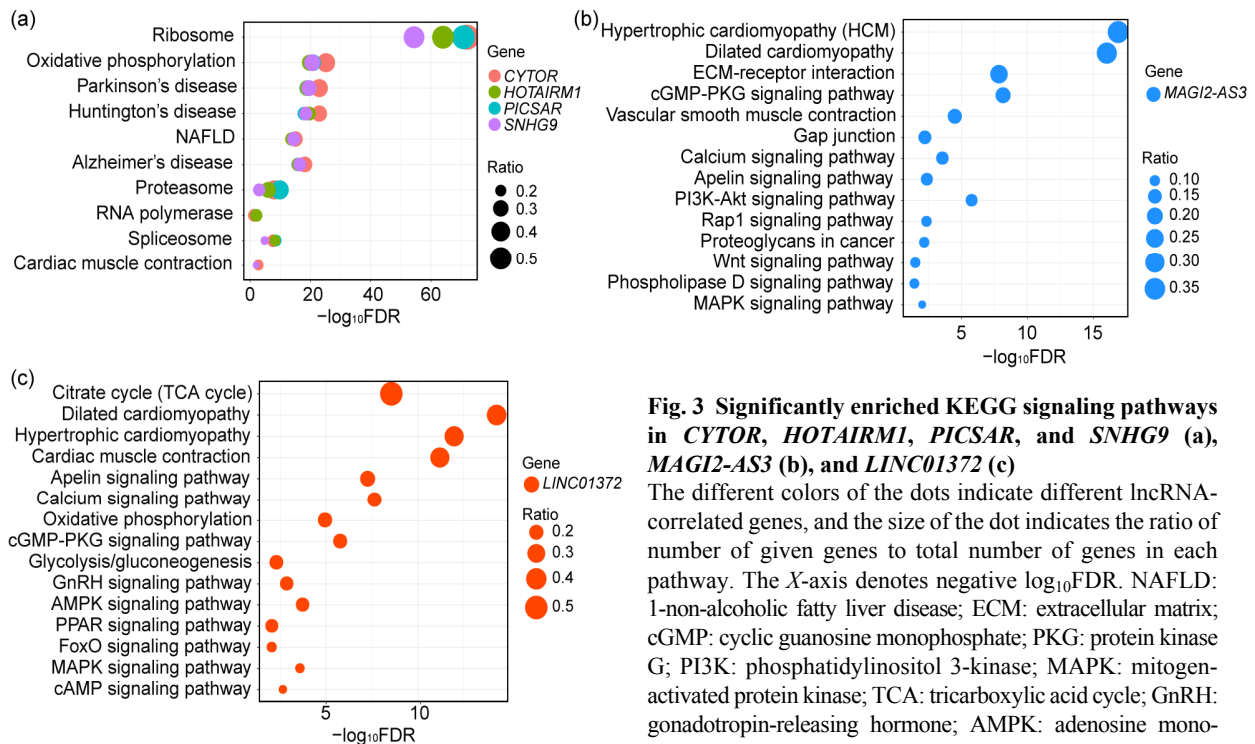
Fig. 3 Significantly enriched KEGG signaling pathways in *CYTOR*, *HOTAIRM1*, *PICSAR*, and *SNHG9* (a), *MAGI2-AS3* (b), and *LINC01372* (c)
The different colors of the dots indicate different lncRNA-correlated genes, and the size of the dot indicates the ratio of number of given genes to total number of genes in each pathway. The X-axis denotes negative $\log_{10}$FDR. NAFLD: 1-non-alcoholic fatty liver disease; ECM: extracellular matrix; cGMP: cyclic guanosine monophosphate; PKG: protein kinase G; PI3K: phosphatidylinositol 3-kinase; MAPK: mitogen-activated protein kinase; TCA: tricarboxylic acid cycle; GnRH: gonadotropin-releasing hormone; AMPK: adenosine monophosphate (AMP)-activated protein kinase; PPAR: peroxisome proliferator-activated receptor; cAMP: cyclic adenosine monophosphate (Note: for interpretation of the references to color in this figure legend, the reader is referred to the web version of this article)

and some oncogenic signaling pathways (calcium, mitogen-activated protein kinase (MAPK), and peroxisome proliferator-activated receptor (PPAR) signaling pathways). However, *FALEC*, *LOC101928844*, and *HCG22* were not found to be involved in any pathway because there were too few connected genes for enrichment analysis. In summary, the pathway analyses above showed that most of these hub lncRNAs may play key roles in malignancies and disease pathogenesis. Compared to previous observations (Nötzold et al., 2017), some new functions of lncRNAs like *LINC01372* and *MAGI2-AS3* were revealed in this study. These findings for uncharacterized lncRNAs expand our knowledge of the possible roles of lncRNAs in HNSCC.

3.6 Correlations between aberrant expression of hub lncRNAs and HNSCC clinical pathological parameters

To gain deeper insight into the associations between the hub lncRNAs and pathogenesis of cancer, we examined the correlation between the expression levels of these lncRNAs and the patients' clinical features in HNSCC. The complete results are shown in Table S6. In total, six lncRNAs were found to be related to one or several features. For example, recent smokers are prone to have a low *PICSAR* expression level compared to reformed smokers. Patients with a low level of *PICSAR* and a high level of *LINC01372* tend to have a smaller tumor size. Moreover, a high expression of *PICSAR* is negatively correlated with node metastasis. Male patients have high *SNHG9* and *HOTAIRM1* levels. *CYTOR* expression was positively correlated with lymph node metastasis (OR=0.49, 95% CI=0.29–0.82, P=0.007; Fig. 4a). High *HCG22* expression was negatively related with tumor size (OR=1.87, 95% CI=1.10–3.18, P=0.021), and more common among female patients (OR=0.49, 95% CI=0.27–0.91, P=0.023) and patients younger than 65 years old (OR=1.88, 95% CI=1.12–3.15, P=0.018), as shown in Fig. 4b. The co-expression network of these six lncRNAs was visualized with Cytoscape based on the top 50 most connected genes for each lncRNA (Fig. S5, Table S7).
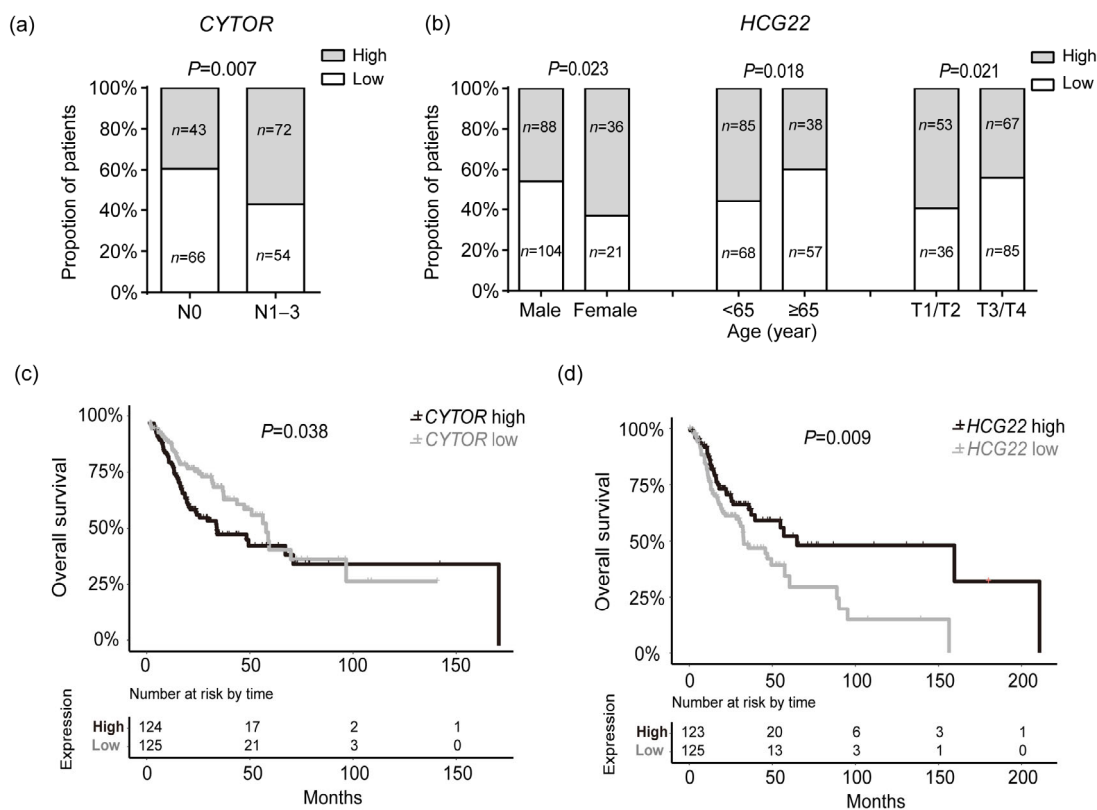
Fig. 4 Clinical feature correlation and survival analysis of potential HNSCC-associated lncRNAs
(a) Correlation of *CYTOR* expression with lymph node metastasis in HNSCC patients. (b) Correlation of *HCG22* expression with gender, age, and tumor size in HNSCC patients. (c, d) Kaplan-Meier analysis of overall survival in HNSCC patients with *CYTOR* (c) and *HCG22* (d) expression. HNSCC patients with higher *HCG22* and lower *CYTOR* expression have a better overall survival. *P*-values were calculated by log-rank test

3.7 *HCG22* and *CYTOR* identified as independent prognostic markers of HNSCC

Cancer biomarker genes usually play important roles in the carcinogenesis of certain cancer types, and contribute to the choice of multiple therapeutic alternatives currently available (Bhatt et al., 2010; Mäbert et al., 2014). We applied Kaplan-Meier analysis to discover candidate lncRNA biomarkers, and a log-rank test to identify the lncRNAs, which led to a significant difference in survival outcome between high and low expression patients. The results indicated that patients with a high *HCG22* expression level (*P*=0.009) and a low *CYTOR* expression level (*P*=0.038) had significantly better OS time (*P*=0.016; Figs. 4c and 4d) and disease free survival (DFS) (*P*=0.001; Figs. S6a and S6b) in a cohort of 500 HNSCC patients. The other four lncRNAs *PICSAR*, *HOTAIRM1*, *SNHG9*, and *LINC01372* did not exhibit

a prognostic ability for HNSCC. Multivariate Cox regression analyses were performed on these two lncRNAs to ensure that their association with patient survival was independent of prognostic factors. As expected, we discovered that the low expression of *CYTOR* could be an independent protective factor for DFS with a hazards ratio of 0.33 and *P*-value of 0.005. *HCG22* was identified as a prognostic factor for both OS (HR=1.68, 95% CI=1.08–2.61, *P*=0.022) and DFS (HR=2.14, 95% CI=1.05–4.38, *P*=0.037), independent of clinical features. The Cox regression analyses of *CYTOR* and *HCG22* are summarized in Table S6. More recently, overexpression of *CYTOR* was reported to be positively correlated with tumor invasion depth, progression, and poor survival in gastric cancer (Chen et al., 2016) and TSCC (Yu et al., 2017), which supports the credibility of our findings. In summary, these findings imply that *CYTOR* might

function as an oncogenic lncRNA and *HCG22* likely acts as a tumor suppressor in HNSCC.

3.8 Validation of the HNSCC lncRNA signature using an independent cohort

To confirm the effectiveness of these nine hub lncRNAs for HNSCC prognosis, we validated their prognostic signatures (only *PICSAR* and *HCG22* were available) on an independent cohort of 81 HNSCC patients from the Oncomine database. We performed clinicopathological parameter analysis, survival analysis, and multivariate Cox regression analysis for these two genes using this dataset. Kaplan-Meier survival analysis indicated that the low expression group of *PICSAR* and *HCG22* was related to poor survival, although *P*-values were larger than 0.05. *HCG22* showed a negative correlation with tumor size (OR=2.89, 95% CI=1.17–7.12, *P*=0.021), and maintained its prognostic value according to multivariate Cox regression analysis in the validation cohort (HR=1.97, 95% CI=1.06–3.64, *P*=0.032). We also analyzed *PICSAR*, but the results were not statistically significant using the analyses mentioned above. The clinical characteristics and Cox regression results for this cohort are listed in Table S8.

3.9 Effect of *CYTOR* knockdown on apoptosis in TSCC15 cells

Our results showed that *CYTOR* was correlated with DNA damage or apoptosis according to GO term enrichment analysis (Table 2). To test the effect of *CYTOR* on tumorigenesis, we performed in vitro apoptosis, EdU, wound healing, and transwell assays on TSCC15 cells. After introducing three *CYTOR* RNA interference (RNAi) products individually into TSCC15 cells, the expression of *CYTOR* was detected by qRT-PCR, which demonstrated a significant decrease in *CYTOR* expression (Fig. S7a). Cisplatin (also named DDP), a platinum-based chemotherapy drug, is one of the most effective drugs used in the treatment of HNSCC (Posner et al., 2007) and dramatically induces cell death. Annexin V+propidium iodide (PI) apoptosis analysis was carried out to measure the amount of apoptotic cells. Our data revealed that the apoptosis rate increased in the presence of 5 µg/ml DDP compared with the control, after *CYTOR* was knocked down (Fig. S7b). EdU, wound healing, and transwell assays were implemented to

assess the effect of *CYTOR* on cell proliferation, mobility, and migration. However, we did not observe a significant difference between the presence of control and indicated *CYTOR* siRNAs in TSCC15 (Figs. S7c–S7e).

4 Discussion

LncRNAs have been increasingly viewed as key factors in various human cancers. Recent studies have established their relationships with gene regulation (Engreitz et al., 2016), epigenetic regulation (Holoch and Moazed, 2015), and cell signaling pathways (Peng et al., 2017). However, the functions of most lncRNAs in cancer have not yet been well characterized. This study focused on identifying HNSCC-associated lncRNAs, and systematically investigating their functions and clinical relevance in HNSCC. Using an integrated approach incorporating differential expression analysis, co-expression network, and gene set enrichment analysis, we discovered nine HNSCC-related lncRNAs. Among them, *FALEC*, *HCG22*, and *LOC101928844* were strongly differentially regulated between HNSCC tumor and adjacent normal tissue, implying that their dysregulation may play a carcinogenic role in cancer development. GO term enrichment analysis based on co-expression network showed that these three lncRNAs were significantly involved in epidermis development and epidermal cell differentiation. Previous studies have shown that *HCG22* expression was reduced in OSCC, and was positively associated with patient survival, but there has been a lack of further functional investigation (Nohata et al., 2016; Feng et al., 2017). In this study, we found that *HCG22* was the most down-regulated lncRNA in HNSCC, and might function in epidermis differentiation. Co-expression network showed that *HCG22* is closely related to EVPL and PPL (Fig. S5). EVPL and PPL are two important proteins in the plakin family, which play a pivotal role in the maintenance of tissue integrity. An earlier study confirmed that EVPL and PPL were down-regulated in HNSCC tissues, which fits with our findings (Chi et al., 2009). We observed that the expression of *HCG22* was negatively correlated with tumor size, and positively correlated with patient OS and DFS. In particular, *HCG22* maintained prognostic significance

independent of clinical features according to multi-variate Cox analysis, which indicated its potential to be an independent prognostic factor in patients with HNSCC. Validation of *HCG22* on an independent cohort showed a similar clinical and prognostic performance, which confirmed our findings.

Based on cancer hallmark, GO term, and KEGG pathway enrichment analysis, *MAGI2-AS3* is relevant mainly to angiogenesis, cell migration, and several cancer-associated signaling pathways, indicating that it might affect the multistep process in tumor progression. *LINC01372* is involved primarily in response to oxygen level, cell development, and hypoxia-related signaling pathways. A large number of findings imply that a local hypoxic microenvironment is one of the most important characteristics of solid tumors (Wilson and Hay, 2011; Eales et al., 2016), suggesting that *LINC01372* may contribute to tumorigenesis. *LINC01372* also showed a positive correlation with tumor size in this study.

Enrichment analysis showed that the connected genes *CYTOR*, *HOTAIRM1*, *SNHG9*, and *PICSAR* are potential *MYC* targets, and are involved in ribosome biogenesis and maintenance of genomic stability. Previous studies have demonstrated that elevated *MYC* expression might lead to genome destabilization in human cancers via coordinating ribosome biogenesis (Wade and Wahl, 2006; Barna et al., 2008). Compelling evidence suggested that *MYC* directly regulates ribosome biogenesis through a multitude of mechanisms (van Riggelen et al., 2010). Dysregulation of ribosome biogenesis is closely associated with alterations in cellular proliferation and apoptosis, and contributes to increasing susceptibility to cancer (Ruggero and Pandolfi, 2003). These findings suggest that *CYTOR*, *HOTAIRM1*, *SNHG9*, and *PICSAR* are closely associated with tumorigenesis. Our in vitro experiments demonstrated that down-regulation of *CYTOR* contributes to TSCC15 cell apoptosis, which is concordant with our co-expression network and functional enrichment analysis. Remarkably, *CYTOR* has a high positive correlation with node metastasis, and a negative correlation with HNSCC patient OS and DFS. Multivariate Cox analysis confirmed that *CYTOR* is an independent predictor of DFS in patients with HNSCC.

In this study, we comprehensively identified HNSCC-associated lncRNAs, and elucidated their biological functions and roles in the oncogenesis of HNSCC. Their prognostic value for patient survival outcome was determined followed by validation on an independent cohort. However, there were some limitations. For example, the tumorigenesis function of the identified lncRNA was tested using cell-based experiments. Further in vivo investigations would be very helpful to fully understand the roles of these lncRNA in TSCC initiation and development. Nevertheless, we are convinced that these findings, based on this large cohort and verified on an independent cohort or by experiments, are valuable not only for fundamental research, but also for potential clinical applications.

5 Conclusions

CYTOR might function in ribosome biogenesis and the maintenance of genomic stability, and had a high positive correlation with node metastasis and a negative correlation with patient OS and DFS. *CYTOR* inhibited cell apoptosis following treatment with the chemotherapeutic drug DDP. *HCG22* might play a role in epidermis differentiation, and was negatively correlated with tumor size and positively correlated with patient OS and DFS. *CYTOR* and *HCG22* were independent prognostic biomarkers for patient outcome. The potential of *HCG22* to be a prognostic biomarker independent of clinical features was validated and confirmed using an external dataset.

References

Aken BL, Ayling S, Barrell D, et al., 2016. The Ensembl gene annotation system. *Database*, 2016:baw093.
https://doi.org/10.1093/database/baw093

Anders S, Pyl PT, Huber W, 2015. HTSeq—a python framework to work with high-throughput sequencing data. *Bioinformatics*, 31(2):166-169.
https://doi.org/10.1093/bioinformatics/btu638

Barna M, Pusic A, Zollo O, et al., 2008. Suppression of Myc oncogenic activity by ribosomal protein haploinsufficiency. *Nature*, 456(7224):971-975.
https://doi.org/10.1038/nature07449

Bartkova J, Hořejší Z, Koed K, et al., 2005. DNA damage

response as a candidate anti-cancer barrier in early human tumorigenesis. *Nature*, 434(7035):864-870.
https://doi.org/10.1038/nature03482

Bartonicek N, Maag JLV, Dinger ME, 2016. Long noncoding RNAs in cancer: mechanisms of action and technological advancements. *Mol Cancer*, 15(1):43.
https://doi.org/10.1186/s12943-016-0530-6

Benjamini Y, Hochberg Y, 1995. Controlling the false discovery rate: a practical and powerful approach to multiple testing. *J Roy Statist Soc B*, 57(1):289-300.

Bhatt AN, Mathur R, Farooque A, et al., 2010. Cancer biomarkers—current perspectives. *Indian J Med Res*, 132:129-149.

Cheetham SW, Gruhl F, Mattick JS, et al., 2013. Long noncoding RNAs and the genetics of cancer. *Br J Cancer*, 108(12):2419-2425.
https://doi.org/10.1038/bjc.2013.233

Chen WM, Huang MD, Sun DP, et al., 2016. Long intergenic non-coding RNA 00152 promotes tumor cell cycle progression by binding to EZH2 and repressing p15 and p21 in gastric cancer. *Oncotarget*, 7(9):9773-9787.
https://doi.org/10.18632/oncotarget.6949

Chi LM, Lee CW, Chang KP, et al., 2009. Enhanced interferon signaling pathway in oral cancer revealed by quantitative proteome analysis of microdissected specimens using ^{16}O/^{18}O labeling and integrated two-dimensional LC-ESI-MALDI tandem MS. *Mol Cell Proteomics*, 8(7):1453-1474.
https://doi.org/10.1074/mcp.M800460-MCP200

de Lena PG, Paz-Gallardo A, Paramio JM, et al., 2017. Clusterization in head and neck squamous carcinomas based on lncRNA expression: molecular and clinical correlates. *Clin Epigenetics*, 9:36.
https://doi.org/10.1186/s13148-017-0334-6

Derrien T, Johnson R, Bussotti G, et al., 2012. The GENCODE v7 catalog of human long noncoding RNAs: analysis of their gene structure, evolution, and expression. *Genome Res*, 22(9):1775-1789.
https://doi.org/10.1101/gr.132159.111

Eales KL, Hollinshead KER, Tennant DA, 2016. Hypoxia and metabolic adaptation of cancer cells. *Oncogenesis*, 5(1): e190.
https://doi.org/10.1038/oncsis.2015.50

Engreitz JM, Ollikainen N, Guttman M, 2016. Long noncoding RNAs: spatial amplifiers that control nuclear structure and gene expression. *Nat Rev Mol Cell Biol*, 17(12):756-770.
https://doi.org/10.1038/nrm.2016.126

Feng L, Houck JR, Lohavanichbutr P, et al., 2017. Transcriptome analysis reveals differentially expressed lncRNAs between oral squamous cell carcinoma and healthy oral mucosa. *Oncotarget*, 8(19):31521-31531.
https://doi.org/10.18632/oncotarget.16358

Gabay M, Li YL, Felsher DW, 2014. MYC activation is a hallmark of cancer initiation and maintenance. *Cold Spring Harb Perspect Med*, 4(6):a014241.
https://doi.org/10.1101/cshperspect.a014241

Geng YJ, Xie SL, Li Q, et al., 2011. Large intervening non-coding RNA HOTAIR is associated with hepatocellular carcinoma progression. *J Int Med Res*, 39(6):

2119-2128.
https://doi.org/10.1177/147323001103900608

Gold KA, Lee HY, Kim ES, 2009. Targeted therapies in squamous cell carcinoma of the head and neck. *Cancer*, 115(5):922-935.
https://doi.org/10.1002/cncr.24123

Hajjari M, Salavaty A, 2015. *HOTAIR*: an oncogenic long non-coding RNA in different cancers. *Cancer Biol Med*, 12(1):1-9.
https://doi.org/10.7497/j.issn.2095-3941.2015.0006

Harrow J, Frankish A, Gonzalez JM, et al., 2012. GENCODE: the reference human genome annotation for the encode project. *Genome Res*, 22(9):1760-1774.
https://doi.org/10.1101/gr.135350.111

Holoch D, Moazed D, 2015. RNA-mediated epigenetic regulation of gene expression. *Nat Rev Genet*, 16(2):71-84.
https://doi.org/10.1038/nrg3863

Huarte M, 2015. The emerging role of lncRNAs in cancer. *Nat Med*, 21(11):1253-1261.
https://doi.org/10.1038/nm.3981

Kassambara A, Kosinski M, 2017. Survminer: Drawing Survival Curves Using 'ggplot2'. R Package Version 0.4.0.
https://CRAN.R-project.org/package=survminer [Accessed on June 10, 2017].

Kim K, Jutooru I, Chadalapaka G, et al., 2013. HOTAIR is a negative prognostic factor and exhibits pro-oncogenic activity in pancreatic cancer. *Oncogene*, 32(13):1616-1625.
https://doi.org/10.1038/onc.2012.193

Kinsella RJ, Kähäri A, Haider S, et al., 2011. Ensembl BioMarts: a hub for data retrieval across taxonomic space. *Database*, 2011:bar030.
https://doi.org/10.1093/database/bar030

Kohl M, Wiese S, Warscheid B, 2011. Cytoscape: software for visualization and analysis of biological networks. In: Hamacher M, Eisenacher M, Stephan C (Eds.), Data Mining in Proteomics. Humana Press, p.291-303.
https://doi.org/10.1007/978-1-60761-987-1_18

Lamouille S, Xu J, Derynck R, 2014. Molecular mechanisms of epithelial-mesenchymal transition. *Nat Rev Mol Cell Biol*, 15(3):178-196.
https://doi.org/10.1038/nrm3758

Langfelder P, Horvath S, 2008. WGCNA: an R package for weighted correlation network analysis. *BMC Bioinform*, 9:559.
https://doi.org/10.1186/1471-2105-9-559

Law CW, Chen Y, Shi W, et al., 2014. voom: precision weights unlock linear model analysis tools for RNA-seq read counts. *Genome Biol*, 15(2):R29.
https://doi.org/10.1186/gb-2014-15-2-r29

LeBleu VS, O'Connell JT, Gonzalez Herrera KN, et al., 2014. PGC-1α mediates mitochondrial biogenesis and oxidative phosphorylation in cancer cells to promote metastasis. *Nat Cell Biol*, 16(10):992-1003.
https://doi.org/10.1038/ncb3039

Leemans CR, Braakhuis BJM, Brakenhoff RH, 2011. The molecular biology of head and neck cancer. *Nat Rev Cancer*, 11(1):9-22.
https://doi.org/10.1038/nrc2982

Li DD, Feng JP, Wu TY, et al., 2013. Long intergenic

noncoding RNA HOTAIR is overexpressed and regulates *PTEN* methylation in laryngeal squamous cell carcinoma. *Am J Pathol*, 182(1):64-70.
https://doi.org/10.1016/j.ajpath.2012.08.042

Li X, Wu Z, Mei Q, et al., 2013. Long non-coding RNA HOTAIR, a driver of malignancy, predicts negative prognosis and exhibits oncogenic activity in oesophageal squamous cell carcinoma. *Br J Cancer*, 109(8):2266-2278.
https://doi.org/10.1038/bjc.2013.548

Liu BD, Sun LJ, Liu Q, et al., 2015. A cytoplasmic NF-κB interacting long noncoding RNA blocks IκB phosphorylation and suppresses breast cancer metastasis. *Cancer Cell*, 27(3):370-381.
https://doi.org/10.1016/j.ccell.2015.02.004

Liu R, Cheng Y, Yu J, et al., 2015. Identification and validation of gene module associated with lung cancer through coexpression network analysis. *Gene*, 563(1):56-62.
https://doi.org/10.1016/j.gene.2015.03.008

Mäbert K, Cojoc M, Peitzsch C, et al., 2014. Cancer biomarker discovery: current status and future perspectives. *Int J Radiat Biol*, 90(8):659-677.
https://doi.org/10.3109/09553002.2014.892229

McCarthy DJ, Chen YS, Smyth GK, 2012. Differential expression analysis of multifactor RNA-Seq experiments with respect to biological variation. *Nucleic Acids Res*, 40(10):4288-4297.
https://doi.org/10.1093/nar/gks042

Miller DL, Davis JW, Taylor KH, et al., 2015. Identification of a human papillomavirus-associated oncogenic miRNA panel in human oropharyngeal squamous cell carcinoma validated by bioinformatics analysis of the cancer genome atlas. *Am J Pathol*, 185(3):679-692.
https://doi.org/10.1016/j.ajpath.2014.11.018

Min SN, Wei T, Wang XT, et al., 2017. Clinicopathological and prognostic significance of homeobox transcript antisense RNA expression in various cancers: a meta-analysis. *Medicine (Baltimore)*, 96(23):e7084.
https://doi.org/10.1097/MD.0000000000007084

Nohata N, Abba MC, Gutkind JS, 2016. Unraveling the oral cancer lncRNAome: identification of novel lncRNAs associated with malignant progression and HPV infection. *Oral Oncol*, 59:58-66.
https://doi.org/10.1016/j.oraloncology.2016.05.014

Nötzold L, Frank L, Gandhi M, et al., 2017. The long non-coding RNA *LINC00152* is essential for cell cycle progression through mitosis in HeLa cells. *Sci Rep*, 7:2265.
https://doi.org/10.1038/s41598-017-02357-0

Parshall MB, 2013. Unpacking the 2×2 table. *Hear Lung J Acute Crit Care*, 42(3):221-226.
https://doi.org/10.1016/j.hrtlng.2013.01.006

Peng WX, Koirala P, Mo YY, 2017. LncRNA-mediated regulation of cell signaling in cancer. *Oncogene*, 36(41):5661-5667.
https://doi.org/10.1038/onc.2017.184

Posner MR, Hershock DM, Blajman CR, et al., 2007. Cisplatin and fluorouracil alone or with docetaxel in head and neck cancer. *New Engl J Med*, 357(17):1705-1715.
https://doi.org/10.1056/nejmoa070956

Pritzker KPH, 2015. Predictive and prognostic cancer biomarkers revisited. *Expert Rev Mol Diagn*, 15(8):971-974.
https://doi.org/10.1586/14737159.2015.1063421

Quek XC, Thomson DW, Maag JLV, et al., 2015. LncRNAdb v2.0: expanding the reference database for functional long noncoding RNAs. *Nucleic Acids Res*, 43(D1):D168-D173.
https://doi.org/10.1093/nar/gku988

R Development Core Team, 2011. R: A Language and Environment for Statistical Computing. R Development Core Team, Vienna, Austria.

Rhodes DR, Yu JJ, Shanker K, et al., 2004. *ONCOMINE*: a cancer microarray database and integrated data-mining platform. *Neoplasia*, 6(1):1-6.
https://doi.org/10.1016/S1476-5586(04)80047-2

Rickman DS, Millon R, de Reynies A, et al., 2008. Prediction of future metastasis and molecular characterization of head and neck squamous-cell carcinoma based on transcriptome and genome analysis by microarrays. *Oncogene*, 27(51):6607-6622.
https://doi.org/10.1038/onc.2008.251

Robinson MD, McCarthy DJ, Smyth GK, 2010. edgeR: a Bioconductor package for differential expression analysis of digital gene expression data. *Bioinformatics*, 26(1):139-140.
https://doi.org/10.1093/bioinformatics/btp616

Ruggero D, Pandolfi PP, 2003. Does the ribosome translate cancer? *Nat Rev Cancer*, 3(3):179-192.
https://doi.org/10.1038/nrc1015

Salazar C, Calvopiña D, Punyadeera C, 2014. miRNAs in human papilloma virus associated oral and oropharyngeal squamous cell carcinomas. *Expert Rev Mol Diagn*, 14(8):1033-1040.
https://doi.org/10.1586/14737159.2014.960519

Salyakina D, Tsinoremas NF, 2016. Non-coding RNAs profiling in head and neck cancers. *NPJ Genomic Med*, 1:15004.
https://doi.org/10.1038/npjgenmed.2015.4

Schmitt AM, Chang HY, 2016. Long noncoding RNAs in cancer pathways. *Cancer Cell*, 29(4):452-463.
https://doi.org/10.1016/j.ccell.2016.03.010

Schmitt AM, Garcia JT, Hung T, et al., 2016. An inducible long noncoding RNA amplifies DNA damage signaling. *Nat Genet*, 48(11):1370-1376.
https://doi.org/10.1038/ng.3673

Seiwert TY, Salama JK, Vokes EE, 2007. The chemoradiation paradigm in head and neck cancer. *Nat Clin Pract Oncol*, 4(3):156-171.
https://doi.org/10.1038/ncponc0750

Signal B, Gloss BS, Dinger ME, 2016. Computational approaches for functional prediction and characterisation of long noncoding RNAs. *Trends Genet*, 32(10):620-637.
https://doi.org/10.1016/j.tig.2016.08.004

Song L, Langfelder P, Horvath S, 2012. Comparison of co-expression measures: mutual information, correlation, and model based indices. *BMC Bioinformatics*, 13:328.
https://doi.org/10.1186/1471-2105-13-328

Subramanian A, Tamayo P, Mootha VK, et al., 2005. Gene set enrichment analysis: a knowledge-based approach for

interpreting genome-wide expression profiles. *Proc Natl Acad Sci USA*, 102(43):15545-15550.
https://doi.org/10.1073/pnas.0506580102

Supek F, Bošnjak M, Škunca N, et al., 2011. REVIGO summarizes and visualizes long lists of gene ontology terms. *PLoS ONE*, 6(7):e21800.
https://doi.org/10.1371/journal.pone.0021800

Therneau T, 2017. A Package for Survival Analysis in S. R Package Version 2.41-2. https://CRAN.R-project.org/package=survival [Accessed on Mar. 20, 2017].

Tsai MC, Manor O, Wan Y, et al., 2010. Long noncoding RNA as modular scaffold of histone modification complexes. *Science*, 329(5992):689-693.
https://doi.org/10.1126/science.1192002

van Riggelen J, Yetil A, Felsher DW, 2010. MYC as a regulator of ribosome biogenesis and protein synthesis. *Nat Rev Cancer*, 10(4):301-309.
https://doi.org/10.1038/nrc2819

Wade M, Wahl GM, 2006. c-Myc, genome instability, and tumorigenesis: the devil is in the details. *Curr Top Microbiol Immunol*, 302:169-203.
https://doi.org/10.1007/3-540-32952-8_7

Wilson WR, Hay MP, 2011. Targeting hypoxia in cancer therapy. *Nat Rev Cancer*, 11(6):393-410.
https://doi.org/10.1038/nrc3064

Yan L, Zhan C, Wu JH, et al., 2016. Expression profile analysis of head and neck squamous cell carcinomas using data from The Cancer Genome Atlas. *Mol Med Rep*, 13(5):4259-4265.
https://doi.org/10.3892/mmr.2016.5054

Yates A, Akanni W, Amode MR, et al., 2016. Ensembl 2016. *Nucleic Acids Res*, 44(D1):D710-D716.
https://doi.org/10.1093/nar/gkv1157

Yu GC, Wang LG, Han YY, et al., 2012. clusterProfiler: an R package for comparing biological themes among gene clusters. *OMICS A J Integr Biol*, 16(5):284-287.
https://doi.org/10.1089/omi.2011.0118

Yu JJ, Liu Y, Guo C, et al., 2017. Upregulated long non-coding RNA LINC00152 expression is associated with progression and poor prognosis of tongue squamous cell carcinoma. *J Cancer*, 8(4):523-530.
https://doi.org/10.7150/jca.17510

Zaidi MR, Davis S, Noonan FP, et al., 2011. Interferon-γ links ultraviolet radiation to melanomagenesis in mice. *Nature*, 469(7331):548-553.
https://doi.org/10.1038/nature09666

Zhang B, Horvath S, 2005. A general framework for weighted gene co-expression network analysis. *Stat Appl Genet Mol Biol*, 4(1):Article 17.
https://doi.org/10.2202/1544-6115.1128

Zhang SC, Tian LL, Ma PH, et al., 2015. Potential role of differentially expressed lncRNAs in the pathogenesis of oral squamous cell carcinoma. *Arch Oral Biol*, 60(10):1581-1587.
https://doi.org/10.1016/j.archoralbio.2015.08.003

Zhao J, Liu YC, Zhang WH, et al., 2015. Long non-coding RNA Linc00152 is involved in cell cycle arrest, apoptosis, epithelial to mesenchymal transition, cell migration and invasion in gastric cancer. *Cell Cycle*, 14(19):3112-3123.
https://doi.org/10.1080/15384101.2015.1078034

List of electronic supplementary materials

中文概要

题　目：头颈部肿瘤转录组分析揭示与核糖体生物合成和表皮分化相关的关键长链非编码 RNA

目　的：研究长链非编码 RNA（lncRNA）与头颈部肿瘤发生、发展及预后的关系。

创新点：通过使用整合的转录组分析方法筛选出与头颈部肿瘤密切相关的 lncRNA，其中 *CYTOR* 和 *HCG22* 在头颈部肿瘤发生发展中具有重要的生物学功能和临床预后价值，为制定新的治疗策略和探索新的预后标记分子提供参考。

方　法：从癌症基因组数据集（The Cancer Genome Atlas）中获得 RNA-seq 数据。结合差异表达分析和共表达网络分析的方法发掘出与头颈部鳞状细胞癌相关的 lncRNA，探讨其与头颈部肿瘤临床病理变化和预后的关系，进一步利用外部数据集以及细胞水平进行验证。

结　论：发现 9 个与头颈部肿瘤发生发展密切相关的 lncRNA，其中 *CYTOR* 可能参与核糖体的生物合成，与病人生存率呈负相关。*HCG22* 可能参与细胞表皮分化过程，与病人生存率呈正相关。此外，*CYTOR* 和 *HCG22* 可作为头颈部鳞状细胞癌独立的预后标记物。

关键词：头颈部肿瘤；长链非编码RNA；加权基因共表达网络分析（WGCNA）；临床病理特征；多因素 Cox回归模型